Neurodegeneration Prevented by Lentiviral Vector Delivery of GDNF in Primate Models of Parkinson's Disease

Jeffrey H. Kordower, *et al.*

Science **290**, 767 (2000);
DOI: 10.1126/science.290.5492.767

Science (print ISSN 0036-8075; online ISSN 1095-9203) is published weekly, except the last week in December, by the American Association for the Advancement of Science, 1200 New York Avenue NW, Washington, DC 20005.

Neurodegeneration Prevented by Lentiviral Vector Delivery of GDNF in Primate Models of Parkinson's Disease

Jeffrey H. Kordower,[1]* Marina E. Emborg,[1] Jocelyne Bloch,[2] Shuang Y. Ma,[1] Yaping Chu,[1] Liza Leventhal,[1] Jodi McBride,[1] Er-Yun Chen,[1] Stéphane Palfi,[1] Ben Zion Roitberg,[1] W. Douglas Brown,[4] James E. Holden,[3,4] Robert Pyzalski,[4] Michael D. Taylor,[3] Paul Carvey,[5] ZaoDung Ling,[5] Didier Trono,[6] Philippe Hantraye,[7] Nicole Déglon,[2] Patrick Aebischer[2,8]

Lentiviral delivery of glial cell line–derived neurotrophic factor (lenti-GDNF) was tested for its trophic effects upon degenerating nigrostriatal neurons in nonhuman primate models of Parkinson's disease (PD). We injected lenti-GDNF into the striatum and substantia nigra of nonlesioned aged rhesus monkeys or young adult rhesus monkeys treated 1 week prior with 1-methyl-4-phenyl-1,2,3,6-tetrahydropyridine (MPTP). Extensive GDNF expression with anterograde and retrograde transport was seen in all animals. In aged monkeys, lenti-GDNF augmented dopaminergic function. In MPTP-treated monkeys, lenti-GDNF reversed functional deficits and completely prevented nigrostriatal degeneration. Additionally, lenti-GDNF injections to intact rhesus monkeys revealed long-term gene expression (8 months). In MPTP-treated monkeys, lenti-GDNF treatment reversed motor deficits in a hand-reach task. These data indicate that GDNF delivery using a lentiviral vector system can prevent nigrostriatal degeneration and induce regeneration in primate models of PD and might be a viable therapeutic strategy for PD patients.

Parkinson's disease is a progressive disorder resulting from degeneration of dopaminergic neurons within the substantia nigra. Surgical therapies aimed at replacing lost dopaminergic neurons or disrupting aberrant basal ganglia circuitry have recently been tested (*1*). However, these clinical trials have focused on patients with advanced disease, and the primary goal of forestalling disease progression in newly diagnosed patients has yet to be realized.

Glial cell line–derived neurotrophic factor (GDNF) has potent trophic effects on dopaminergic nigral neurons (*2–8*), suggesting that this factor could provide neuroprotection in patients with early PD. We have shown that intraventricular administration of GDNF failed to improve clinical function or prevent nigrostriatal degeneration in a patient with PD, and this failure resulted from an ineffective delivery method (*9*). Gene therapy is a powerful means to deliver trophic molecules to the central nervous system in a site-specific manner. Robust transfer of marker and therapeutic genes has recently been demonstrated in the rodent and nonhuman primate brain with the use of a lentiviral vector (*10–15*). The transgene expression is long-term and nontoxic. Using two different nonhuman primate models of PD, we examined whether lentiviral-mediated delivery of GDNF could reverse the cellular and behavioral changes associated with nigrostriatal degeneration in primates. For the first model, we chose nonlesioned aged monkeys that displayed a slow progressive loss of dopamine within the striatum and tyrosine hydroxylase (TH) within the substantia nigra without frank cellular degeneration (*16*). These aged monkeys demonstrate changes within the nigrostriatal system that model some of the incipient cellular changes seen in early PD (*17*). In the second model, young adult monkeys received unilateral intracarotid injections of 1-methyl-4-phenyl-1,2,3,6-tetrahydropyridine (MPTP) to induce extensive nigrostriatal degeneration, resulting in a behavioral syndrome characterized by robust motor deficits.

In the first experiment, eight aged (approximately 25 years old) female rhesus monkeys received injections of lentiviral vectors encoding β-galactosidase (lenti-βGal; $n = 4$) or GDNF (lenti-GDNF; $n = 4$) targeted for the striatum and substantia nigra (*18*) and were killed 3 months later. Postmortem, all GDNF injections were localized to the caudate nucleus, putamen, and supranigral regions (*19*), as revealed by standard staining procedures (*20*). All aged monkeys receiving lenti-GDNF displayed robust GDNF immunoreactivity within the right striatum (Fig. 1A) and substantia nigra (Fig. 1C). In contrast, no monkeys receiving lenti-βGal displayed specific GDNF immunoreactivity in the right striatum (Fig. 1B). Rather, these monkeys displayed robust expression of βGal similar to that reported previously (*15*). In lenti-GDNF–treated animals, GDNF immunoreactivity within the striatum was extremely dense and distributed throughout the neuropil (Fig. 1). When the primary antibody concentration was decreased to one-tenth of the standard, the intense striatal neuropil staining was diminished, and GDNF-immunoreactive perikarya were easily seen. Numerous GDNF-immunoreactive perikarya were also seen within the substantia nigra of lenti-GDNF–injected monkeys. Within the striatum and substantia nigra, Nissl-stained sections revealed normal striatal cytoarchitecture without significant cytotoxicity. Macrophages were occasionally observed within the needle tracts. Gliosis was similar across treatment groups and was principally confined to the regions immediately surrounding the needle tracts.

Lenti-GDNF injections resulted in marked anterograde transport of the trophic factor. Intense GDNF immunoreactivity was observed within fibers of the globus pallidus (Fig. 1D) and substantia nigra pars reticulata (Fig. 1E) after striatal injections. GDNF-containing fibers emanating from putaminal injection sites were seen coursing medially toward and into the globus pallidus (Fig. 1D). These staining patterns were clearly distinct from the injection site and respected the boundaries of the striatal target structures. In contrast, anterograde transport of βGal was not observed in lenti-βGal monkeys. This suggests that secreted GDNF, and not the virus per se, was anterogradely transported.

Aged monkeys underwent fluorodopa (FD) positron emission tomography (PET) before surgery and again just before being killed (*21*). Before treatment, all monkeys displayed symmetrical FD uptake in the caudate and putamen bilaterally (ratio: 1.02 ± 0.02) (Figs. 2A and 2B, left). Similarly, there was symmetrical (4% difference) FD uptake in all lenti-βGal–treated monkeys after lentivirus injections (Fig. 2A, right). In contrast, FD uptake was significantly asymmetrical

[1]Department of Neurological Sciences and [5]Department of Pharmacology, Rush Presbyterian–St. Luke's Medical Center, Chicago, IL 60612, USA. [2]Division of Surgical Research and Gene Therapy Center, Lausanne University Medical School, Lausanne, Switzerland. [3]Department of Medical Physics and [4]Department of Radiology, University of Wisconsin, Madison, WI 53706, USA. [6]Department of Genetics and Microbiology, Faculty of Medicine, University of Geneva, Geneva, Switzerland. [7]Commissariat a l'Energie Atomique (CEA), CNRS, Unite de Recherche Associe (URA), 2210 Service Hospitalier Frederic Joliot, CEA, Direction des Sciences du Vivant (DSV), Departement de Recherche Medicale (DRM), Orsay cedex, France. [8]Swiss Federal Institute of Technology, EPFL, Lausanne, Switzerland.

*To whom correspondence should be addressed. E-mail: jkordowe@rush.edu

(27%) in lenti-GDNF–treated monkeys with greater uptake on the side of the GDNF expression ($P < 0.007$; Fig. 2B, right). With respect to absolute values, lenti-βGal animals displayed a trend toward reduced FD uptake after treatment relative to baseline levels ($P = 0.06$). Qualitatively, three of four lenti-GDNF–treated monkeys displayed clear increases in FD uptake on the treated side. This increase in uptake (K_i value) between the groups just failed to reach statistical significance ($P = 0.06$).

Within the striatum, lentiviral delivery of GDNF increased a number of markers of dopaminergic function (*22*). Optical density measurements were performed to assess the relative intensity of TH staining within the caudate nucleus and putamen (Fig. 3, A and B). On the left side where there was no lenti-GDNF expression, the intensity of TH immunoreactivity within the caudate nucleus and putamen was similar between groups (Fig. 3, A and B). In contrast, significant increases in optical density measures of TH immunoreactivity were seen in the right striatum of lenti-GDNF–infused monkeys (Fig. 3A) relative to lenti-βGal–treated animals (Fig. 3B) or the contralateral side (Fig. 3A). In this regard, there was a 44.1% and a 38.9% increase in optical density measures of TH immunoreactivity within the caudate nucleus and putamen, respectively (Fig. 4D). At the time of death, tissue punches were taken throughout the caudate nucleus and putamen of all monkeys. Relative to lenti-βGal–treated animals, measurement of dopamine (DA) and homovanillic acid (HVA) revealed significant increases in the right caudate nucleus (140% DA, $P < 0.001$; 207% HVA, $P < 0.001$) and putamen (47.2% DA, $P < 0.05$; 128% HVA, $P < 0.01$) in lenti-GDNF–treated aged monkeys (Fig. 4, E and F).

Lentiviral delivery of GDNF to aged monkeys resulted in an increase in the number of TH-immunoreactive neurons within the substantia nigra (Fig. 3, C and D). Regardless of the extent of GDNF immunoreactivity within the midbrain, the organization of TH-immunoreactive neurons was similar in all animals, and these neurons were not observed in ectopic locations within this locus. Stereological counts revealed an 85% increase in the number of TH-immunoreactive nigral neurons on the side receiving lentivirally delivered GDNF (Fig. 4A) relative to lenti-βGal–treated animals. On the side (left) that did not display GDNF immunoreactivity, lenti-GDNF–treated animals contained 76,929 ± 4918 TH-immunoreactive neurons. This is similar to what was seen in lenti-βGal–infused animals (68,543 ± 5519). Whereas lenti-βGal–infused monkeys contained 63,738 ± 6094 TH-immunoreactive nigral neurons in the right side, lenti-GDNF–treated monkeys contained 118,170 ± 8631 TH-immunoreactive nigral neurons in this hemisphere ($P < 0.001$).

A similar pattern was seen when the volume of TH-immunoreactive substantia nigra neurons was quantified (Fig. 4B). TH-immunoreactive neurons from lenti-βGal– and lenti-GDNF–treated monkeys were similar in size in the left nigra where there was no GDNF expression (11,147.5 ± 351 μm^3 and 11,458.7 ± 379 μm^3, respectively). In contrast, a 35% increase in neuronal volume was seen on the GDNF-rich right side in lenti-GDNF–injected aged monkeys (lenti-βGal 10,707.5 ± 333 μm^3; lenti-GDNF 16,653.7 ± 1240 μm^3; $P < 0.001$).

Although stereological counts of TH mRNA–containing neurons were not performed, there was an obvious increase in the number of TH mRNA–containing neurons within the right substantia nigra in lenti-GDNF–treated monkeys (Fig. 3E) compared with lenti-βGal–containing animals (Fig. 3F). With regard to the relative levels of TH mRNA expression within individual nigral neurons (*23*), the pattern of results was similar to that observed with TH-immunoreactive neuronal number and volume (Fig. 4C). On the left side, the optical density of TH mRNA within nigral neurons was similar between lenti-βGal– and lenti-GDNF–treated monkeys (78.28 ± 2.78 and 80.58 ± 2.5, respectively). In contrast, there was a significant (21.5%) increase in the optical density for TH mRNA in lenti-GDNF–treated monkeys (98.3 ± 1.5) relative to lenti-βGal–treated monkeys (77.2 ± 2.3) on the right side ($P < 0.01$).

In the second experiment, 20 young adult rhesus were initially trained 3 days per week until asymptotic performance was achieved on a hand-reach task in which the time to pick up food treats out of recessed wells was measured (*16*, *24*). Each experimental day, monkeys received 10 trials per hand. Once per week, monkeys were also evaluated on a modified parkinsonian clinical rating scale

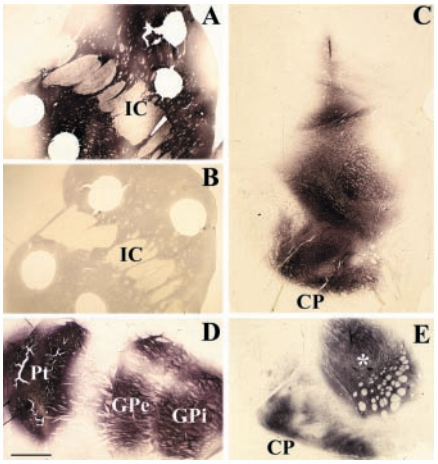

Fig. 1. (**A**) Dense GDNF immunoreactivity within the head of the caudate nucleus and putamen in a lenti-GDNF–treated aged monkey. (**B**) In contrast, no GDNF immunoreactivity was observed in these regions in a lenti-βGal–treated animal. IC, internal capsule. (**C**) Dense GDNF immunoreactivity was observed within the midbrain of a lenti-GDNF–treated animal. (**D**) GDNF immunoreactivity within the forebrain of a lenti-GDNF–treated monkey. The staining within the putamen (Pt) is from an injection site. The staining within both segments of the globus pallidus (GPe and GPi) is the result of anterograde transport. (**E**) Anterogradely transported GDNF was also seen in the substantia nigra pars reticulata. Note that the holes in the tissue sections were made post mortem for HPLC analysis. Asterisk in (E) represents a lenti-GDNF injection site (CP, cerebral peduncle). Scale bar in (D) represents 1600 μm for panels A, B, and D; 1150 μm for panel C, and 800 μm for panel E.

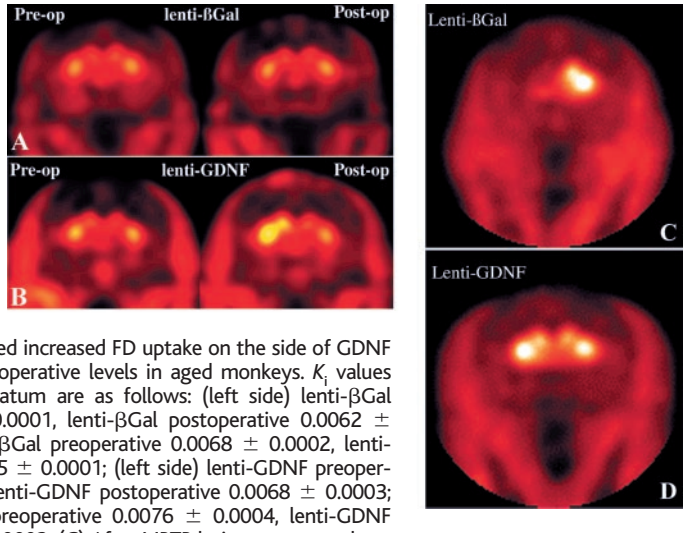

Fig. 2. PET scan data evaluating the influence of lenti-GDNF on FD uptake in (A and B) intact aged monkeys and (C and D) young adult MPTP-treated monkeys. (**A**) FD uptake did not change from baseline to 3 months after lentivirus injection in lenti-βGal–treated aged monkeys. (**B**) In contrast, lenti-GDNF injections manifested increased FD uptake on the side of GDNF expression relative to preoperative levels in aged monkeys. K_i values (per minute) for the striatum are as follows: (left side) lenti-βGal preoperative 0.0068 ± 0.0001, lenti-βGal postoperative 0.0062 ± 0.0002; (right side) lenti-βGal preoperative 0.0068 ± 0.0002, lenti-βGal postoperative 0.0065 ± 0.0001; (left side) lenti-GDNF preoperative 0.0072 ± 0.0005, lenti-GDNF postoperative 0.0068 ± 0.0003; (right side) lenti-GDNF preoperative 0.0076 ± 0.0004, lenti-GDNF postoperative 0.0081 ± 0.0003. (**C**) After MPTP lesions, a comprehensive loss of FD uptake was seen within the right striatum of lenti-βGal–treated young adult monkeys. (**D**) In contrast, FD uptake was enhanced in lenti-GDNF–treated monkeys. K_i values (per minute) for the striatum are as follows: lenti-βGal left, 0.0091 ± 0.0004; lenti-βGal right, 0.0017 ± 0.0005; lenti-GDNF left, 0.0084 ± 0.0004; lenti-GDNF right, 0.0056 ± 0.0018.

(CRS). All monkeys then received an injection of 3 mg MPTP-HCl into the right carotid artery, initiating a parkinsonian state. One week later, monkeys were evaluated on the CRS. Only monkeys displaying severe hemiparkinsonism with the classic crooked arm posture and dragging leg on the left side continued in the study ($n = 10$). It is our experience that monkeys with this behavioral phenotype display the most severe lesions neuroanatomically and do not display spontaneous recovery behaviorally (*24*). On the basis of CRS scores, monkeys were matched into two groups of five monkeys, which received on that day lenti-βGal or lenti-GDNF treatment. Using magnetic resonance imaging (MRI) guidance, we gave all monkeys lentivirus injections into the caudate nucleus ($n = 2$), putamen ($n = 3$), and substantia nigra ($n = 1$) on the right side using the same injection parameters as in experiment 1. One week later, monkeys began retesting on the hand-reach task three times per week for 3 weeks per month (*25*). For statistical analyses, the times for an individual week were combined into a single score. During the weeks of hand-reach testing, monkeys were also scored once per week on the CRS. Individuals blinded to the experimental treatment performed all behavioral assessments. Three months after lentivirus treatment, monkeys received a FD PET scan and were killed 24 to 48 hours later, and tissues were histologically processed as before.

Within 1 week after the lentivirus injections, one monkey from each group died. Necropsies from these animals revealed only the presence of mild necrosis from multifocal random hepatocellular coagulation. On account of these deaths, all remaining monkeys underwent detailed necropsies after death, and no significant abnormalities in any organs were seen.

Before MPTP treatment, all young adult monkeys scored 0 on the CRS. After MPTP, but before lentivirus injection, monkeys in the lenti-GDNF and lenti-βGal groups averaged 10.4 ± 0.07 and 10.6 ± 0.6, respectively, on the CRS ($P > 0.05$). After lentivirus treatment, significant differences in CRS scores were seen between the two groups (Kolmogorov-Smirnov test, $P < 0.0001$; Fig. 5A). CRS scores of monkeys receiving lenti-βGal did not change over the 3-month period after treatment. In contrast, CRS scores of monkeys receiving lenti-GDNF significantly diminished during the 3-month period after treatment. Scores began to decrease in the first month after lenti-GDNF treatment. However, statistically significant differences between lenti-GDNF and lenti-βGal were only discerned at posttreatment observations 6, 7, 8, and 9 (Kolmogorov-Smirnov test, $P < 0.04$ for each comparison).

Lenti-GDNF–treated animals also improved performance on the operant hand-reach task. Under the conditions before MPTP administration, animals in both groups performed this task with similar speed (Fig. 5B). For the "unaffected" right hand, no differences in motor function were discerned for either group relative to performance before MPTP administration or to each other ($P > 0.05$). In contrast, performance with the left hand was significantly improved in lenti-GDNF–treated animals relative to controls ($P < 0.05$). After MPTP, all lenti-βGal–treated animals were severely impaired, with monkeys often not performing at all, or requiring more than the maximally allowed 30 s. In contrast, three of the four lenti-GDNF monkeys performed the task with the left hand at near-normal levels, whereas one lenti-GDNF–treated monkey was impaired and performed this task in a manner similar to the lenti-βGal–treated animals. Between groups, significant differences in performance were discerned on posttreatment tests 4, 6, 7, 8, and 9 ($P < 0.05$ for each comparison).

Just before being killed, all monkeys underwent FD PET scans. Qualitatively, all lenti-βGal–treated monkeys displayed pro-

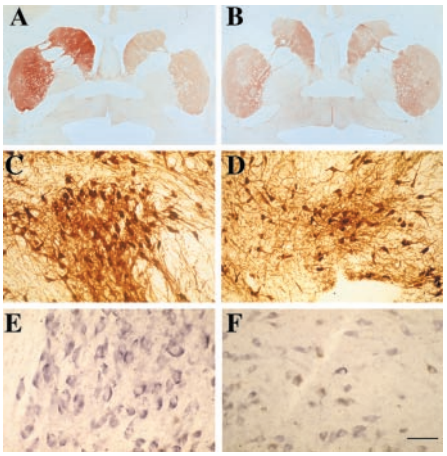

Fig. 3. (**A**) Section stained for TH immunoreactivity through the anterior commissure illustrating the increase in TH immunoreactivity within the right caudate nucleus and putamen after lenti-GDNF delivery to aged monkeys. (**B**) Symmetrical and less intense staining for TH immunoreactivity in a monkey injected with lenti-βGal. (**C**) There were greater numbers and larger TH-immunoreactive neurons within the substantia nigra of a lenti-GDNF–treated animal relative to (**D**) a lenti-βGal–treated monkey. (**E**) Lenti-GDNF–treated aged monkeys displayed increased TH mRNA relative to (**F**) lenti-βGal–treated monkeys in the SN. Scale bar in (F) represents 4500 μm for panels 250 μm for panels (C) and (D) and 100 μm for panels (E) and (F).

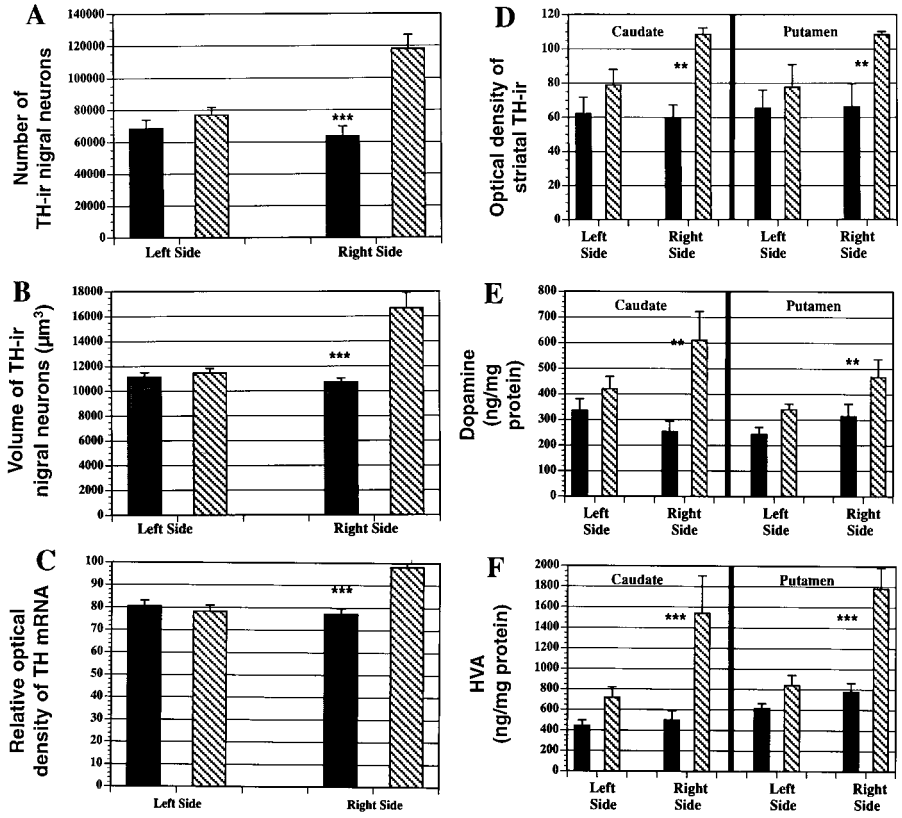

Fig. 4. (**A** through **F**) Plots of quantitative data illustrating enhanced nigrostriatal function in lenti-GDNF–treated aged monkeys. Solid bars denote lenti-βGal–treated monkeys; hatched bars indicate lenti-GDNF–treated monkeys. GDNF expression was limited to the right striatum and nigra. $^{**}P < 0.01$; $^{***}P < 0.001$.

nounced FD uptake in the left striatum and a comprehensive loss of FD uptake on the right side (Fig. 2C). In contrast, two of four lenti-GDNF–treated animals displayed robust and symmetrical FD uptake on both sides (Fig. 2D). The remaining two lenti-GDNF monkeys displayed reduced FD uptake on the right side, but with K_i values 50 to 100% greater than lenti-βGal controls (Fig. 2). Quantitatively, no differences in FD uptake were observed between groups within the left striatum ($P > 0.05$). In contrast, there was a significant (>300%) increase in FD uptake in lenti-GDNF–treated animals in the right striatum relative to lenti-βGal–treated animals ($P < 0.05$). When the right striatum was subdivided, significant increases in FD uptake were only seen within the putamen of lenti-GDNF–treated animals ($P < 0.05$).

After death, a strong GDNF-immunoreactive signal was seen in the caudate nucleus, putamen, and substantia nigra of all lenti-GDNF–treated, but none of the lenti-βGal–treated animals. The intensity and distribution of GDNF immunoreactivity was indistinguishable from what we observed in aged monkeys (see Fig. 1).

All lenti-βGal–treated monkeys displayed a comprehensive loss of TH immunoreactivity within the striatum on the side ipsilateral to the MPTP injection (Fig. 6A). In contrast, all lenti-GDNF–treated monkeys displayed enhanced striatal TH immunoreactivity relative to βGal controls (Fig. 6B). However, there was variability in the degree of striatal TH immunoreactivity in lenti-GDNF–treated animals and that variability was associated with the degree of functional recovery seen on the hand-reach task. Two lenti-GDNF–treated monkeys displayed dense TH immunoreactivity throughout the rostrocaudal extent of the striatum (Fig. 6B). In these monkeys, the intensity of the TH immunoreactivity was greater than that observed on the intact side. These two animals displayed the best functional recovery. A third lenti-GDNF–treated monkey also displayed robust functional recovery on the hand-reach task. However, the enhanced striatal TH immunoreactivity in this animal was limited to the post-commissural putamen. The fourth lenti-GDNF–treated monkey did not recover on the hand-reach task. Although putaminal TH immunoreactivity in this animal was still greater than controls, the degree of innervation was sparse and restricted to the medial post-commissural putamen.

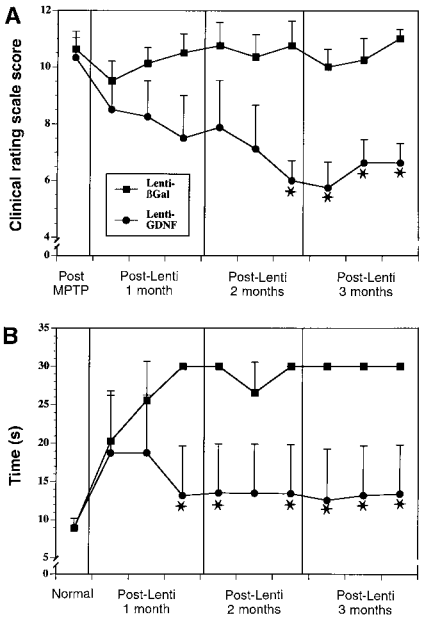

Fig. 5. After MPTP-treatment, lenti-GDNF–injected monkeys displayed functional improvement on (**A**) the clinical rating scale and (**B**) the hand-reach task. All tests were performed 3 weeks per month [see (*15*)]. On the clinical rating scale, monkeys were matched into groups based upon the post-MPTP score. For the hand-reach task, each symbol represents the mean of three sessions per week for the left hand. Monkeys were not tested on this task during the week between MPTP and lentivirus injection. *$P < 0.05$ relative to lenti-βGal.

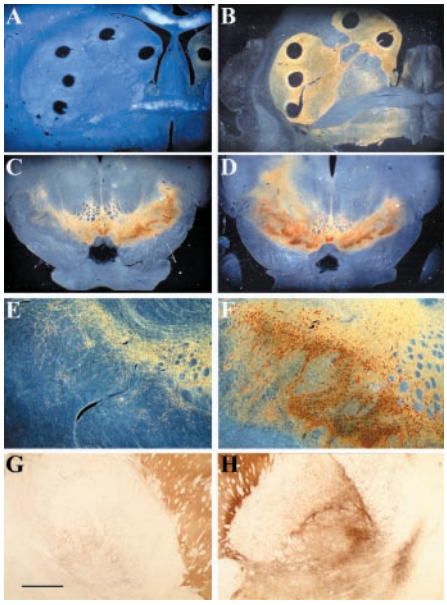

Fig. 6. (**A** and **B**) Low-power dark-field photomicrographs through the right striatum of TH-immunostained sections of MPTP-treated monkeys treated with (A) lenti-βGal or (B) lenti-GDNF. (A) There was a comprehensive loss of TH immunoreactivity in the caudate and putamen of lenti-βGal–treated animal. In contrast, near normal level of TH immunoreactivity is seen in lenti-GDNF–treated animals. Low-power (**C** and **D**) and medium-power (**E** and **F**) photomicrographs of TH-immunostained section through the substantia nigra of animals treated with lenti-βGal (C and E) and lenti-GDNF (D and F). Note the loss of TH-immunoreactive neurons in the lenti-βGal–treated animals on the side of the MPTP-injection. TH-immunoreactive sprouting fibers, as well as a supranormal number of TH-immunoreactive nigral perikarya are seen in lenti-GDNF–treated animals on the side of the MPTP injection. (**G** and **H**) Bright-field low-power photomicrographs of a TH-immunostained section from a lenti-GDNF–treated monkey. (G) Note the normal TH-immunoreactive fiber density through the globus pallidus on the intact side that was not treated with lenti-GDNF. (H) In contrast, an enhanced network of TH-immunoreactive fibers is seen on the side treated with both MPTP and lenti-GDNF. Scale bar in (G) represents the following magnifications: (A), (B), (C), and (D) at 3500 μm; (E), (F), (G), and (H) at 1150 μm.

Lenti-GDNF treatment enhanced the expression of TH-immunoreactive fibers throughout the nigrostriatal pathway. Unlike what was observed in aged monkeys, however, some TH-immunoreactive fibers in the striatum displayed a morphology characteristic of both degenerating and regenerating fibers. Large, thickened fibers could be seen coursing in an irregular fashion in these animals. Rostrally, these fibers appeared disorganized at times, with a more normal organization seen more caudally. TH-immunoreactive sprouting was also seen in the globus pallidus (Fig. 6, G and H), substantia innominata (Fig. 6, A and B), and lateral septum. These novel staining patterns were not immunoreactive for dopamine β-hydroxylase confirming the dopaminergic phenotype of this response.

Quantitatively, lenti-βGal–treated monkeys displayed significant decreases in the optical density of TH-immunoreactive fibers within the right caudate nucleus (71.5%; $P < 0.006$; Fig. 7D) and putamen (74.3% $P < 0.0007$; Fig. 7D) relative to the intact side. When analyzed as a group, TH optical density in the right caudate nucleus and putamen of lenti-GDNF–treated monkeys was significantly greater than that seen in lenti-βGal–treated monkeys ($P < 0.001$ for both) and was similar to that seen on the intact side of these animals ($P > 0.05$ for both).

All lenti-βGal–treated monkeys displayed a dramatic loss of TH-immunoreactive neurons within the substantia nigra on the side ipsilateral to the MPTP injection (Fig. 7A). In contrast, the nigra from all four of the lenti-GDNF–treated displayed complete neuroprotection (Fig. 7A), regardless of the degree of functional recovery. In lenti-βGal–treated monkeys, intracarotid injections of MPTP resulted in an 89% decrease in the number (Fig. 7A), and an 81.6% decrease in the density, of TH-immunoreactive nigral neurons on the side ipsilateral to the toxin injection ($P < 0.001$). In contrast, lenti-GDNF–treated monkeys displayed 32% more TH-immunoreactive nigral neurons ($P < 0.001$) and an 11% increase in TH-immunoreactive neuronal density ($P < 0.05$) relative to the intact side. In lenti-βGal–treated animals, MPTP significantly reduced (32%) the volume of residual TH-immunoreactive nigral neurons on the lesion side relative to the intact side ($P < 0.001$; Fig. 7B). In contrast, the volume of

TH-immunoreactive neurons in lenti-GDNF–treated animals was significantly larger (44.3%) on the lesioned side relative to the intact side ($P < 0.001$). Finally, the optical density of TH mRNA was quantified bilaterally in all animals (Fig. 7C). In lenti-βGal–treated animals, there was a significant decrease (24.0%) in the relative optical density of TH mRNA within residual neurons on the MPTP-lesioned side relative to the intact side ($P < 0.03$). In contrast, lenti-GDNF–treated animals displayed a significant increase (41.7%) in relative optical density of TH mRNA relative to the intact side or lenti-βGal–treated animals ($P < 0.001$).

Sections from all monkeys were stained for CD45, CD3, and CD8 markers to assess the immune response after lentiviral vector injection (*26*). These antibodies are markers for activated microglia, T cells, and leukocytes including lymphocytes, monocytes, granulocytes, eosinophils, and thymocytes. Staining for these immune markers was weak, and often absent, in these animals. Mild staining for CD45 and CD8 was seen in two animals. Some CD45-immunoreactive cells displayed a microglial morphology. Other monkeys displayed virtually no immunoreactivity even in sections containing needle tracts.

Two additional intact young adult rhesus monkeys received lenti-GDNF injections into the right caudate and putamen and the left substantia nigra using the same injection protocol (*26*). These animals were killed 8 months later and were evaluated by immunohistochemistry and enzyme-linked immunosorbent assay (ELISA) (*27*) for long-term gene expression. Robust GDNF immunoreactivity was seen in the right caudate, right putamen, and left ventral midbrain in both animals. In the right substantia nigra, many GDNF-immunoreactive neurons were seen. This labeling represents retrograde transport of GDNF after injections of lenti-GDNF into the right striatum. Further, dense GDNF-immunoreactive fiber staining, representing anterograde transport of the trophic factor, was seen within the right substantia nigra pars reticulata. Tissue punches taken at the time of death revealed significant levels of GDNF produced by striatal cells 8 months after lenti-GDNF injections. On the side without a striatal injection, 0.130 ± 0.062 and 0.131 ± 0.060 ng/mg protein of GDNF were seen in the caudate nucleus and putamen, respectively. Significantly higher GDNF levels were observed within the caudate nucleus (2.25 ± 0.312 ng/mg protein; $P < 0.001$) and putamen (3.5 ± 0.582 ng/mg protein; $P < 0.001$) on the lenti-GDNF–injected side.

Our study demonstrates that delivery of GDNF cDNA into the nigrostriatal system using a lentiviral vector system can potently reverse the structural and functional effects of dopamine insufficiency in nonhuman primate models of aging and early Parkinson's disease. Most critically, lenti-GDNF delivery prevented the motor deficits that normally occur after MPTP administration. In this regard, functional disability was prevented on both a subjective clinical rating scale modeled after the Unified Parkinson's Disease Rating Scale and an objective operant motor test. Consistent expression of GDNF was observed in aged and lesioned monkeys with significant and biologically relevant levels of GDNF observed for up to 8 months after lentivirus injection. Indeed, the 2.5 to 3.5 ng/mg protein of GDNF produced after lenti-GDNF injections compares very favorably to the 50 to 152 pg/mg protein of striatal GDNF produced after intrastriatal adenovirus injections in monkeys (*28*).

This consistent gene expression occurred without significant toxicity to aged monkeys, and minor toxicity in two of the MPTP-treated monkeys, supporting our previous observations (*15*). Still, the death of two monkeys needs to be addressed. Pathological analyses revealed only a mild necrosis from multifocal random hepatocellular coagulation in these animals, and this was not deemed to be the cause of death. No other young adult or aged monkeys from this or a previous study (*15*) displayed morbidity or mortality after lentivirus injections. Further, detailed necropsies from the remaining MPTP-treated animals failed to reveal any relevant pathology. Although the absolute cause of death remains elusive, we hypothesize that the death of these two monkeys relates to the impact of the surgical procedure 1 week after the MPTP injections and is unrelated to the lentivirus injection.

In aged monkeys, lentiviral delivery of GDNF augmented host nigrostriatal function as determined by a variety of morphological, physiological, and neurochemical dependent measures. In this regard, lenti-GDNF increased the size and number of TH-immunoreactive neurons within the substantia nigra; increased the expression of TH mRNA within these neurons; increased the levels of dopamine, dopaminergic metabolites, and dopaminergic markers in the striatum; and increased FD uptake within the striatum as determined by PET scan. Enhanced nigrostriatal dopamine function was consistently associated with the expression of lentivirally delivered GDNF, as enhanced nigrostriatal function was only seen on the side with robust gene expression.

We used aged monkeys to model specific cellular changes that occur in aging and the earliest aspects of PD. Phenotypic down-regulation of the TH gene and protein are among the earliest pathological events seen within the substantia nigra in PD (*17*), and analogous changes are seen in aged rhesus monkeys (*16*). The number of TH-immunoreactive nigral neurons seen in lenti-βGal–injected animals was similar to that previously reported for aged rhesus monkeys (*16*). In contrast, lenti-GDNF–treated aged monkeys displayed nigral neurons in numbers similar to those seen in young adult animals. The possibility that the lenti-GDNF spurred neurogenesis of dopaminergic nigral neurons cannot be ruled out. However, the delivery of lenti-GDNF to the nigral region resulted in transgene expression throughout the midbrain. Yet, TH-immunoreactive neurons were observed only within established catecholaminergic nuclei and not in ectopic midbrain locations. A more parsimonious explanation is that

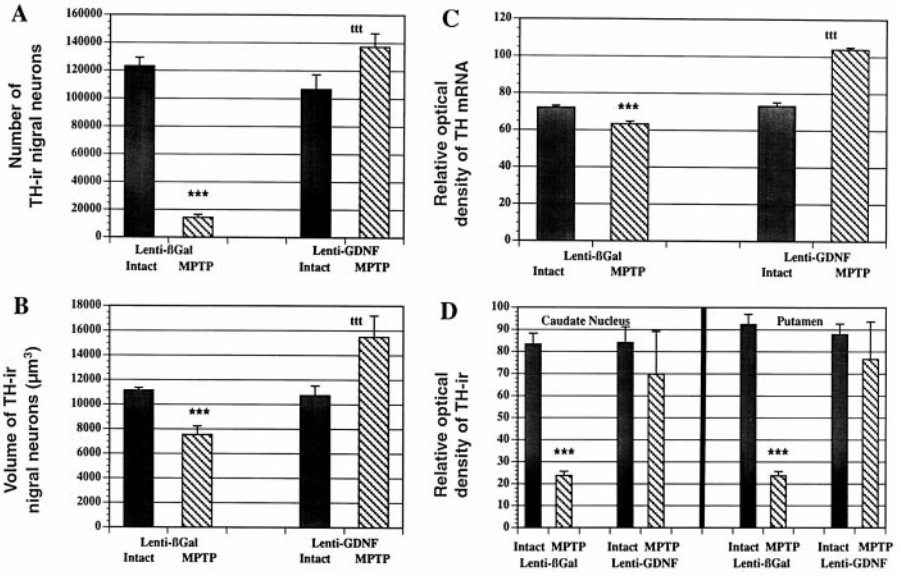

Fig. 7. (**A** through **D**) Quantification of lenti-GDNF's trophic effects on nigral neuronal number, volume, TH mRNA and striatal TH immunoreactivity in MPTP-treated monkeys. ***$P < 0.001$ significant decreases relative to intact side; ttt denotes significant increases relative to the intact side.

GDNF up-regulated TH-immunoreactivity in aged nigral neurons that had previously down-regulated TH expression below detectable levels. The enhanced TH mRNA expression seen within nigral neurons after lenti-GDNF treatment supports this interpretation.

Lenti-GDNF also prevented the behavioral and neuroanatomical effects of MPTP-induced nigrostriatal degeneration. It is notable that, unlike many other neuroprotection paradigms, the lenti-GDNF injections were performed after the parkinsonian state was initiated, thus better modeling what can be attempted in PD patients. The exact mechanism by which lenti-GDNF exerted its effects requires further elucidation. It is clear that neuroprotection was achieved within the substantia nigra, as these neurons do not degenerate within a week of MPTP treatment (*29*). However, striatal fibers can degenerate during this time, and whether the GDNF is preventing degeneration or inducing sprouting of degenerating fibers still needs to be established. Indeed, there is evidence for both mechanisms as some animals displayed fiber morphology and topography indicative of regeneration.

A critical question is whether preservation of striatal innervation, nigral perikarya, or both, is required for functional recovery. Although the number of animals in our study is too small to provide a definitive answer, it is notable that all lenti-GDNF–treated monkeys had complete preservation of nigral perikarya. Yet, functional recovery on the hand-reach task was absent only in the one monkey with sparsest striatal reinnervation. Thus it appears that GDNF-mediated striatal reinnervation is critical for functional recovery in nonhuman primates, a concept supported by recent studies performed in rodents (*30*, *31*). The failure to potently protect dopaminergic innervation in the one monkey may be due to variability in the speed by which nigrostriatal fibers are lost after MPTP. At the time of the lenti-GDNF injections, dopaminergic fibers in this monkey may have regressed to a level where access to the GDNF was limited, and regrowth to the striatum was impossible.

Not only was lenti-GDNF capable of preventing the degeneration of nigrostriatal neurons in MPTP-treated monkeys, it augmented many of the morphological parameters relative to the "intact" side. It is likely that the unilateral 3-mg MPTP dose induced a small loss of TH-immunoreactive neurons on the contralateral side. Thus the increased numbers of TH-immunoreactive neurons may reflect complete neuroprotection on the side of GDNF expression contrasted with a small loss of TH-immunoreactive neurons on the side not injected.

We injected lentivirus into both the striatum and substantia nigra in order to maximize the chance for an effect. For lenti-GDNF therapy to be a practical clinical approach, studies determining the regions of GDNF delivery critical to reverse progressive nigrostriatal degeneration are needed. The importance of related biological events such as anterograde transport of GDNF from injection sites to target regions also needs to be established. Finally, potential adverse events resulting from lenti-GDNF inducing supranormal levels of striatal dopamine needs to be evaluated. Toward this end, vectors with built-in inducible systems that can modulate gene expression in cases of dose-limiting side effects need to be developed. Still, the reversal of slowly progressive cellular phenotypic changes seen in aged monkeys, combined with the structural and functional neuroprotection and regeneration seen in MPTP-treated monkeys, indicates that lentiviral delivery of GDNF may provide potent clinical benefits for patients with PD.

References and Notes

1. C. Honey, R. E. Gross, A. M. Lozano, *Can. J. Neurol. Sci.* **2**, S45 (1999).
2. A. Björklund, C. Rosenblad, C. Winkler, D. Kirik, *Neurobiol. Dis.* **4**, 196 (1997).
3. J. L. Tseng, E. E. Baetge, A. D. Zurn, P. Aebischer, *J. Neurosci.* **17**, 325 (1997).
4. P. A. Lapchak, D. M. Gash, S. Jiao, P. J. Miller, D. Hilt, *Exp. Neurol.* **144**, 29 (1997).
5. D. M. Gash, G. A. Gerhardt, B. J. Hoffer, *Adv. Pharmacol.* **42**, 11 (1998).
6. C. M. Kearns, D. M. Gash, *Brain Res.* **672**, 104 (1995).
7. D. L. Choi-Lundberg *et al.*, *Science* **275**, 838 (1997).
8. D. M. Gash *et al.*, *Nature* **380** 252 (1996).
9. J. H. Kordower *et al.*, *Ann. Neurol.* **46**, 419 (1999).
10. L. Naldini *et al.*, *Science*, **272**, 263 (1996).
11. M. Takahashi, H. Miyoshi, I. M. Verma, F. H. Gage, *J. Virol.* **73**, 7812 (1999).
12. K. A. Mitrophanous *et al.*, *Gene Ther.* **6**, 1808 (1999).
13. G. Wang *et al.*, *J. Clin. Invest.* **104**, 55 (1999).
14. N. Déglon *et al.*, *Hum. Gene Ther.* **11**, 179, (2000).
15. J. H. Kordower *et al.*, *Exp. Neurol.* **160**, 1 (1999).
16. M. E. Emborg *et al.*, *J. Comp. Neurol.* **401**, 253 (1998).
17. A. Kastner, E. C. Hirsh, Y. Agid, F. Javoy Agid, *Brain Res.* **606**, 341 (1993).
18. The cDNA coding for a nuclear-localized β-galactosidase (LacZ) and the human GDNF containing a Kozak consensus sequence (a 636-bp fragment: position 1 to 151 and 1 to 485; GenBank accession numbers L19062 and L19063) were cloned in the SIN-W-PGK transfer vector [R. Zufferey *et al.*, *J. Virol.* **73**, 2886 (1999)]. The packaging construct and vesicular stomatis virus G protein (VSV-G) envelope used in this study were the PCMVDR8.92, PRSV-Rev, and the PMD.6 plasmids described previously; R. Zufferey, D. Nagy, R. J. Mandel, L. Naldini, D. Trono, *Nature Biotechnol.* **15**, 871 (1997); A. F. Hottinger, M. Azzouz, N. Déglon, P. Gebischer, A. D. Zurn, *J. Neurosci.* **20**, 5587 (2000). The viral particles were produced in 293T cells as previously described (*15*). The titers (3 to 5 $\times$ 10^8 TU/ml) of the concentrated LacZ-expressing viruses (200,000 and 250,000 ng p24/ml in experiment 1 and 450,000 ng p24/ml in experiment 2) were determined on 293T cells. The GDNF-expressing viral stocks were normalized for viral particles content using p24 antigen measurement.
19. All experimentation was performed in accordance with NIH guidelines and institutional animal care approval. Level II Biosafety procedures were used. Under MRI guidance, each monkey received six stereotaxic injections of lenti-βGal or lenti-GDNF bilaterally into the caudate nucleus, putamen, and substantia nigra. Injections were made into the head of the caudate nucleus (10 μl), body of the caudate nucleus (5 μl), anterior putamen (10 μl), commissural putamen (10 μl), postcommissural putamen (5 μl), and substantia nigra (5 μl). Injections were made through a 10-μl Hamilton syringe connected to a pump at a rate of 0.5 μl/min. During the injection, the needle was raised 1 to 2 mm to better disperse the lentivirus through the intended target. The needle was left in place for an additional 3 min to allow the injectate to diffuse from the needle tip. The left side was injected 6 weeks before the right. During the first surgical session, there was a technical failure with the virus aggregating in the needle, which prevented its injection into the brain. This was confirmed at postmortem examination using GDNF-immunohistochemistry and βGal histochemistry. Thus, the left side served as an additional control for the right side.
20. GDNF immunohistochemistry was performed with a commercially available antibody (R&D Systems, Minneapolis, MN; 1:250), using the ABC method and nickel intensification. Deletion or substitution for the primary antibody served as controls. Under control conditions, no staining was observed.
21. All procedures followed an overnight fast. After sedation with ketamine (10 to 15 mg/kg), the animal was intubated, and femoral angiocatheters were placed for tracer injection and blood sampling. Anesthesia was then maintained by 1 to 2% isofluorane for the remainder of the procedure. Carbidopa (2 to 3 mg/kg IV) was administered 30 min before the FD study. The animal was placed in a stereotaxic head holder constructed of materials compatible with PET scanning, and a transmission scan was acquired for correction of the emission data for attenuation. FD (185 MBq) was administered over 30 s and a 90-min three-dimensional dynamic emission scan started. The scan included 22 frames with durations increasing from 1 min initially to 5 min at the end. The bed was moved cyclically by the interplane distance between each pair of 5-min scans to give a net coronal sampling interval of 2.125 mm. Regions of interest (ROI) were placed on the caudate nucleus, putamen and occipital cortex in individual morphometric MR images coregistered with the FD image data. Cortical time courses were used as input functions to generate functional maps of the uptake rate constant K_i by the modified graphical method [C. S. Patlak, R. G. Blasberg, *J. Cereb. Blood Flow Metab.* **5**, 584 (1985)]. Striatal ROIs were transferred to the functional maps, and the K_i values were evaluated as the ROI means for each structure.
22. All monkeys were perfused with saline. The brain was removed, immersed in ice-cold saline for 10 min, and slabbed on a monkey brain slicer. Slabs through the head of the caudate and putamen were punched bilaterally with a 1-mm brain punch. These punches were processed for HPLC (*24*). The tissue slabs were immersed in Zamboni's fixative. Stereological counts and volumes of TH-immunoreactive neurons were performed with NeuroZoom software using the optical dissector method for cell counting and the nucleator method for measuring neuronal volume (*16*).
23. The TH riboprobe was prepared as previously described (*9*). The probe was conjugated to 2 mM biotin-14-CTP (Gibco BRL/Life Technologies, Rockville, MD), 1 μg Pvu I–linearized pBS-TH3′, 5 mM DTT, 50 U RNasin, 4 U T3RNA polymerase, 0.5 mM CTP, and 0.25 mM of ATP, GTP, and UTP. Tissue was processed for immunohistochemistry by the ABC method using this probe as the primary antibody. Optical density measurements were performed using NIH Image.
24. J. H. Kordower, *Cell Transplant.* **4**, 155 (1995).
25. Testing was performed during weeks 2 to 4 for month 1, and weeks 1 to 3 for months 2 and 3. Monkeys were not tested for the first week in month 1 to allow them time to recover from surgery. Testing was not performed for the final week of months 2 and 3 to allow for routine veterinary care (month 2) and transportation to the University of Wisconsin for PET scans (month 3).
26. Supplementary material, Web figures 1 and 2, is available to *Science* Online subscribers www.sciencemag.org/feature/data/1047824.shl
27. Brain punches were homogenized in 150:1 buffer I [0.1M tris-buffered saline, pH 8.1, containing 1 mM EDTA, 1% aprotinin, 10 μg/ml leupeptin, 14 μg/ml pepstatin, 4 mM phenylmethylsulfonyl fluoride (PMSF)] for 30 s in the ice slurry. An equal amount of buffer II (0.1 M tris-buffered saline, pH 8.1, containing 1 mM EDTA, 1% aprotinin, 10 g/ml leupeptin, 14

μg/ml pepstatin, 4 mM PMSF, and 0.5% NP-40) was then added. The tubes were shaken for 2 hours in the The supernatant was collected for ELISA and protein measurements. The ELISA reaction was completed in 96-well plate (Dynatech, Chantilly, VA) according to the ELISA manufacturer's instructions (GDNF E_{max} ImmunoAssay Systems Kit G3520, Promega, Madison, WI). The optical densities were recorded in ELISA plate reader (at 450 nm wave length; Dynatech). Some lysates were diluted to ensure all the optical densities were within the standard curve. The concentrations or GDNF were calculated against six-point standard curve and then adjusted to picograms of GDNF per milligram of total protein. The total protein in each tissue lysate was measured using Bio-Rad protein assay kit (Bio-Rad, Richmond, CA).

28. D. A. Kozlowski *et al*., ASNTR, Abstr. **7**, 25 (2000).
29. J. L. Eberling *et al*., *Brain Res.* **832**, 184 (1999).
30. B. Connor *et al*., *Gene Ther.* **6**, 1936 (1999).
31. C. Rosenblad, D. Kirik, A. Björklund, *Exp. Neurol.* **16**, 503 (2000).

32. This research was supported by a grant from the Department of Defense, The Charles Shapiro Foundation, NS40578, and by the Swiss National Science Foundation and the Swiss National Program in Neurological Diseases. We thank T. Collier for comments on this manuscript, T. Kladis and J. Stansell for expert histological assistance, F. Pidoux and M. Rey for the technical assistance in the production of the lentiviral vectors, K. Gibbons for assistance with PET scans, and J. Sladek Jr. for photographic assistance.

9 December 1999; accepted 17 August 2000

Quantum Superposition of Macroscopic Persistent-Current States

Caspar H. van der Wal,[1]* A. C. J. ter Haar,[1] F. K. Wilhelm,[1] R. N. Schouten,[1] C. J. P. M. Harmans,[1] T. P. Orlando,[2] Seth Lloyd,[3] J. E. Mooij[1,2]

Microwave spectroscopy experiments have been performed on two quantum levels of a macroscopic superconducting loop with three Josephson junctions. Level repulsion of the ground state and first excited state is found where two classical persistent-current states with opposite polarity are degenerate, indicating symmetric and antisymmetric quantum superpositions of macroscopic states. The two classical states have persistent currents of 0.5 microampere and correspond to the center-of-mass motion of millions of Cooper pairs.

When a small magnetic field is applied to a superconducting loop, a persistent current is induced. Such a persistent supercurrent also occurs when the loop contains Josephson tunnel junctions. The current is clockwise or counterclockwise, thereby either reducing or enhancing the applied flux to approach an integer number of superconducting flux quanta Φ_0 (*1*). In particular when the enclosed magnetic flux is close to half-integer values of Φ_0, the loop may have multiple stable persistent-current states, with at least two of opposite polarity. The weak coupling of the Josephson junctions then allows for transitions between the states. Previous theoretical work (*2*–*4*) proposed that a persistent current in a loop with Josephson junctions corresponds to the center-of-mass motion of all the Cooper pairs in the system and that quantum mechanical behavior of such persistent-current states would be a manifestation of quantum mechanical behavior of a macroscopic object. In a micrometer-sized loop, millions of Cooper pairs are involved. At very low temperatures, excitations of individual charge carriers around the center of mass of the Cooper-pair condensate are prohibited by the superconducting gap. As a result, the coupling between the dynamics of persistent supercurrents and many-body quasi-particle states is very weak. Josephson junction loops therefore rank among the best objects for experimental tests of the validity of quantum mechanics for systems containing a macroscopic number of particles (*3*, *5*, *6*) [loss of quantum coherence results from coupling to an environment with many degrees of freedom (*7*)] and for research on the border between classical and quantum physics. The potential for quantum coherent dynamics has stimulated research aimed at applying Josephson junction loops as basic building blocks for quantum computation (qubits) (*8*–*11*).

We present microwave spectroscopy experiments that demonstrate quantum superpositions of two macroscopic persistent-current states in a small loop with three Josephson junctions (Fig. 1A). At an applied magnetic flux of $\frac{1}{2}\Phi_0$, the system behaves as a particle in a double-well potential, where the classical states in each well correspond to persistent currents of opposite sign. The two classical states are coupled via quantum tunneling through the barrier between the wells, and the loop is a macroscopic quantum two-level system (Fig. 1B) (*12*). The energy levels vary with the applied flux as shown (Fig. 1C). Classically, the levels cross at $\frac{1}{2}\Phi_0$. Tunneling between the wells leads to quantum mechanical eigenstates that at $\frac{1}{2}\Phi_0$ are symmetric and antisymmetric superpositions of the two classical persistent-current states. The symmetric superposition state is the quantum mechanical ground state with an energy lower than the classical states; the antisymmetric superposition state is the loop's first excited state with an energy higher than the classical states. Thus, the superposition states manifest themselves as an anticrossing of the loop's energy levels near $\frac{1}{2}\Phi_0$. We performed spectroscopy on the loop's two quantum levels (Fig. 2) and our results show the expected anticrossing at $\frac{1}{2}\Phi_0$ (Fig. 3) (*13*). We also studied the resonance-line shapes and found behavior similar to microscopic quantum two-level systems (*14*, *15*) (Fig. 4).

Detecting quantum superposition. In our experiments, the magnetic flux generated by the loop's persistent current was measured with an inductively coupled direct-current superconducting quantum interference device (DC-SQUID) (Figs. 1 and 2), while low-amplitude microwaves were applied to induce transitions between the levels. We observed narrow resonance lines at magnetic field values where the level separation ΔE was resonant with the microwave frequency. The DC-SQUID performs a measurement on a single quantum system. Thus, we should expect that the measurement process limits the coherence of our system. While the system is pumped by the microwaves, the SQUID actively measures the flux produced by the persistent currents of the two states. Detecting the quantum levels of the loop is still possible because the meter is only weakly coupled to the loop. The flux signal needs to be built up by averaging over many repeated measurements on the same system (Fig. 2B), such that an ensemble average is effectively determined. We measure the level separation, i.e., energy rather than flux, as we perform spectroscopy, and we observe a change in averaged flux when the microwaves are resonant with the level separation (the peaks and dips in Figs. 2B and 3A). We also chose to work with an extremely underdamped DC-SQUID with unshunted junctions to minimize damping of the quantum system via the inductive coupling to the SQUID.

Similar observations were recently made by Friedman *et al.* (*16*) who performed spectroscopy on excited states in a loop with a

[1]Department of Applied Physics and Delft Institute for Micro Electronics and Submicron Technology (DIMES), Delft University of Technology, Post Office Box 5046, 2600 GA Delft, Netherlands. [2]Department of Electrical Engineering and Computer Science and [3]Department of Mechanical Engineering, Massachusetts Institute of Technology, Cambridge, MA 02139, USA.

*To whom correspondence should be addressed. E-mail: caspar@qt.tn.tudelft.nl